

Asymptotic motion of a single vortex in a rotating cylinder

J.M. Karimäki^{*,†}, R. Hänninen^{*}, and E.V. Thuneberg[†]

^{*}*O.V. Lounasmaa Laboratory, Aalto University, P.O. Box 15100, FI-00076 AALTO, Finland and*

[†]*Department of Physics, University of Oulu, Oulu, Finland*

(Dated: April 8, 2013)

We study numerically the behavior of a single quantized vortex in a rotating cylinder. We study in particular the spiraling motion of a vortex in a cylinder that is parallel to the rotation axis. We determine the asymptotic form of the vortex and its axial and azimuthal propagation velocities under a wide range of parameters. We also study the stability of the vortex line and the effect of tilting the cylinder from the rotation axis.

I. INTRODUCTION

Since the discovery of quantized vortices, the motion of those vortices under various conditions has attracted continued attention of researchers¹⁻⁷. In recent years emphasis has been shifting to the study of the so-called quantum turbulence and numerical simulations with a large number of vortices⁸⁻¹⁴. This requires a considerable amount of computing power, especially when calculations are performed using the full Biot-Savart equations³. There is, however, still a need to better understand the motion of a single vortex. Since the motion of a curved vortex line is somewhat counter-intuitive, and solving the equations analytically is difficult and prone to errors, it is convenient to use numerical simulations. For single vortices, it also becomes a realistic possibility to scan a large volume of parameter space, i.e. various combinations of pressure p , temperature T , rotational velocity Ω , vessel size and shape, and initial vortex configurations.

An existing computer software, previously used mainly for studying the large scale behavior of many vortices¹⁵⁻¹⁷, is applied to study the motion of a single vortex line. More specifically, we study the motion of a single superfluid vortex filament in a rotating infinite cylinder, as illustrated in Figs. 1 and 2. This case has recently been studied using analytic approximations in Ref. 18. A closely related problem, where a wire is placed on the axis of the cylinder, has been studied earlier¹⁹⁻²².

Our main point of interest is the asymptotic velocity of the vortex end touching the side wall of the cylinder. We calculate the evolution of the vortex from the initial state using the vortex filament model of the two-fluid paradigm with Biot-Savart formalism, until the asymptotic situation is reached. We assume the normal fluid component of the velocity to be in rigid body rotation. Although we have used ³He-B-specific parameters in our calculations, the methods and the results can be generalized to vortices in other superfluids and Bose-Einstein condensates in many cases.

One surprising effect discovered in our calculations is the stability of the vortex, even in the low temperature limit. This contradicts the expectations based especially on experimental results in ³He-B^{13,23}. We assume that the discrepancy with experiments is caused by some surface effects not accounted for in our model (such as pinning), or due to some uncontrolled heat leaks or superflows that may destabilize the vortices in the experiments.

II. MODEL

We study a superfluid in an infinite cylinder of radius R that rotates at constant angular velocity Ω . For the most part in this paper the axis of rotation is assumed to be the cylinder axis. The effects caused by a rotation axis that is tilted with respect to the cylinder axis are considered in Secs. VI and VII at the end of the paper. We use cylindrical coordinates (r, ϕ, z) fixed to the cylinder. Our study is based on the two-fluid model, where the normal and superfluid components have velocities \mathbf{v}_n and \mathbf{v}_s , respectively. The normal component is assumed to be in rigid body rotation, $\mathbf{v}_n = \Omega \times \mathbf{r}$. This is a good assumption in ³He-B, because mutual friction is weak in comparison to the viscosity of the normal fluid⁴.

The superfluid velocity \mathbf{v}_s is determined by vortex lines³. The positions on the vortex lines are given by $\mathbf{s}(\xi, t)$, which is parametrized by the vortex length ξ and time t . (The direction in which ξ increases conforms to the right-hand rule for the superfluid circulation around the vortex.) Partial derivatives with respect to ξ are denoted by primes. Then, the unit tangent of the vortex core line is the first derivative of \mathbf{s} with respect to ξ . This is denoted by \mathbf{s}' (or $\hat{\mathbf{s}}'$ to emphasize that it is a unit vector). The superfluid velocity \mathbf{v}_s is calculated using the (full) Biot-Savart formalism:

$$\mathbf{v}_s(\mathbf{r}, t) = \mathbf{v}_\omega + \mathbf{v}_b, \quad (1)$$

with

$$\mathbf{v}_\omega = \frac{\kappa}{4\pi} \int_{\mathcal{L}} \frac{(\mathbf{s}_1 - \mathbf{r}) \times d\mathbf{s}_1}{|\mathbf{s}_1 - \mathbf{r}|^3}, \quad (2)$$

where \mathcal{L} denotes all the vortex lines and κ is the circulation of the superfluid velocity around a vortex line; all the positions and velocities are in laboratory coordinates. The first term, \mathbf{v}_ω , in Eq. (1) needs to be numerically calculated from the integral (2). It has a divergence on the vortex core, which has to be cut off at the vortex core radius²⁴ a , see Refs. 3 and 25 for details. The second term, \mathbf{v}_b , is the boundary field, or image velocity field, needed to prevent flow across the vessel boundary. The boundary field \mathbf{v}_b can be calculated from the Laplace equation, or by the method of image vortices. To calculate \mathbf{v}_b we use the method of approximate image vortices as in Ref. 25.

The derivative of $\mathbf{s}(\xi, t)$ with respect to time defines the vortex line velocity \mathbf{v}_L except that the component of \mathbf{v}_L parallel to the line is not defined. The equation of motion is commonly

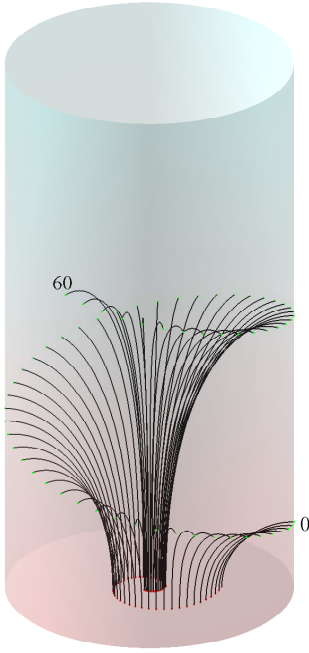


FIG. 1. (Color online) The evolution of a vortex in a rotating coordinate system. The total time span $2.79/\alpha\Omega$ comprises 61 snapshots. Other parameters are $\text{Re}_\alpha = 3.63$ ($\sim 0.4T_c$ in $^3\text{He-B}$) and $2\pi R^2\Omega/\kappa = 85.5$.

written in laboratory coordinates as³:

$$\mathbf{v}_L = \mathbf{v}_s + \alpha \hat{\mathbf{s}}' \times (\mathbf{v}_n - \mathbf{v}_s) - \alpha' \hat{\mathbf{s}}' \times [\hat{\mathbf{s}}' \times (\mathbf{v}_n - \mathbf{v}_s)]. \quad (3)$$

It contains the mutual friction parameters α and α' . They depend on temperature and pressure, but the temperature dependence is usually much stronger, e.g., in the case of superfluid $^3\text{He-B}$ the temperature dependence is dramatic^{26,27}. A useful new quantity involving α and α' can be defined as $\text{Re}_\alpha := (1 - \alpha')/\alpha$. It has some similarity with the Reynolds number defined in normal fluids^{23,28,29}. In $^3\text{He-B}$ the quantity $\text{Re}_\alpha(T)$ decreases monotonically from ∞ to 0, when the temperature increases from 0 to T_c . Furthermore, the experimentally accessible range of Re_α in $^3\text{He-B}$ essentially covers this whole range. Table I contains some approximative values of the parameters α , α' , and Re_α , as functions of temperature.

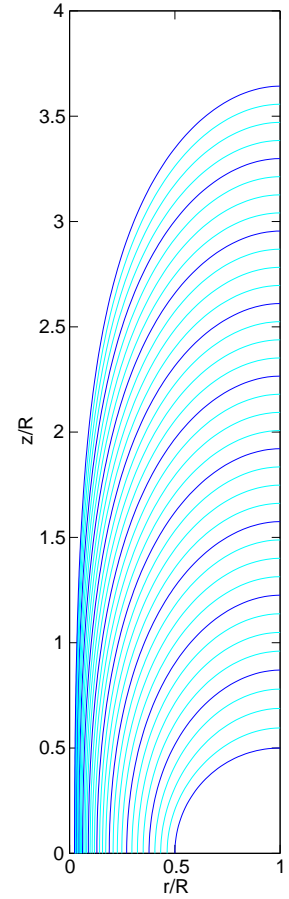
Using the fact that the normal component is in rigid body motion ($\mathbf{v}_n = \Omega \times \mathbf{r}$ in the laboratory coordinates), we can rewrite the equation of motion (3) in rotating coordinates (where $\mathbf{v}_n = 0$) as:

$$\mathbf{v}_L = \alpha(\text{Re}_\alpha \mathbf{v}_s - \hat{\mathbf{s}}' \times \mathbf{v}_s). \quad (4)$$

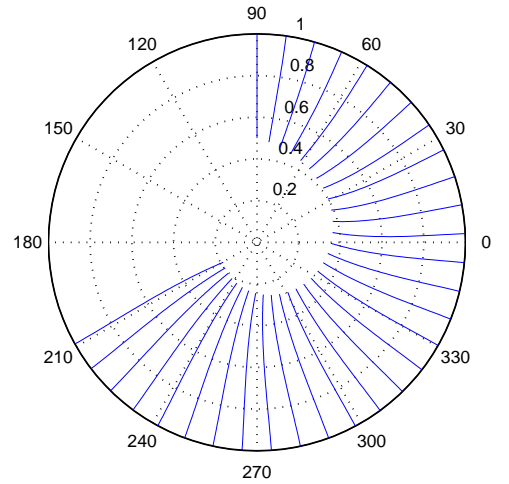
From now on all velocities will be in rotating coordinates, unless explicitly stated otherwise.

We study in particular the velocity of the vortex end in the long-time limit ($t \rightarrow \infty$). For that we define v_{Lz} and $v_{L\phi}$ by writing in the rotating frame:

$$\mathbf{v}_L = v_{Lz} \hat{\mathbf{e}}_z + v_{L\phi} \hat{\mathbf{e}}_\phi. \quad (5)$$



a)



b)

FIG. 2. (Color online) The evolution of the vortex shown in Fig. 1 presented in cylindrical coordinates fixed to the rotating frame. a) (r, z) plot with 37 snapshots in time span $4.19/\alpha\Omega$. b) Polar plot with 31 snapshots in time span $1.40/\alpha\Omega$.

It is also possible to define the climbing angle β of the vortex in the rotating frame by $\tan \beta = v_{Lz}/v_{L\phi}$. The climbing angle in the laboratory frame satisfies $\tan \beta = v_{Lz}/(v_{L\phi} + R\Omega)$.

T/T_c	α	α'	Re_α
0.00	0	0	∞
0.25	1.265828E-02	5.255042E-03	7.858453E+01
0.30	4.701086E-02	3.032361E-02	2.062665E+01
0.35	1.200093E-01	8.150743E-02	7.653512E+00
0.40	2.328964E-01	1.556440E-01	3.625457E+00
0.45	3.467192E-01	2.429385E-01	2.183500E+00
0.50	4.565632E-01	3.333683E-01	1.460108E+00
0.55	5.620771E-01	4.201522E-01	1.031616E+00
0.60	6.732573E-01	4.999895E-01	7.426737E-01
0.65	8.104478E-01	5.719796E-01	5.281283E-01
0.70	1.004341E+00	6.365370E-01	3.618920E-01
0.75	1.295975E+00	6.946998E-01	2.355757E-01
0.80	1.736739E+00	7.478107E-01	1.452085E-01
0.85	2.448636E+00	7.974992E-01	8.269943E-02
1.00	∞	1	0

TABLE I. Tabulated values of α , α' , and Re_α used in the numerical calculations. These values approximately correspond to those in $^3\text{He-B}$ at 29.34 bar at the temperatures shown on the left. The limit values of the parameters at $T = 0$ and $T = T_c$ are also shown.

III. SCALING PROPERTIES

The parameter space of the system (without considering the parameters describing the initial vortex configuration) consists of mutual friction parameters α and α' , the vortex core radius a , the circulation quantum κ , the cylinder radius R , the angular velocity Ω , and for a tilted cylinder the tilting angle θ . The exploration of this parameter space is simplified by dimensional analysis. Let us, for example, study the asymptotic axial velocity v_{Lz} (5) of the vortex end in the absence of tilting, $\theta = 0$. According to dimensional analysis, the dimensionless velocity $v_{Lz}/R\Omega$ can only depend on dimensionless quantities appearing in the problem, which in this case are R/a , $R^2\Omega/\kappa$, α , and α' . Thus the parameter space is four-dimensional. Using properties specific to the present problem, we show in the following that this space can further be reduced to three dimensions exactly and to two dimensions approximately.

Let us consider the evolution of a vortex state from a fixed initial configuration. We see from Eq. (4) that varying α but keeping Re_α constant has the effect of changing the time scale only.³⁰ This means that the dimensionless time is $\alpha\Omega t$ and the dimensionless line velocity is $\mathbf{v}_L/\alpha R\Omega$, but otherwise there is no dependence on α . (Note that the dimensionless superfluid velocity $\mathbf{v}_s/R\Omega$ does not have α .) Since the asymptotic velocity is obtained in the limit $t \rightarrow \infty$, the dependence on $\alpha\Omega t$ drops out. Since the system is dissipative (for $\alpha \neq 0$), the same final state can be obtained by a variety of initial states, i.e. the details of the initial state are not important either. Thus we conclude that the asymptotic velocity has the form

$$v_{Lz} = \alpha R \Omega G_z \left(\frac{R^2 \Omega}{\kappa}, \frac{R}{a}, \frac{1 - \alpha'}{\alpha} \right), \quad (6)$$

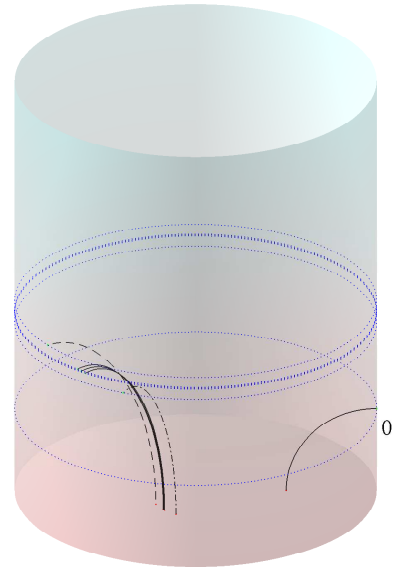


FIG. 3. (Color online) The effect of the parameter R/a . The solid lines have R/a equal to 1, 0.5, and 0.25 times 1.77×10^5 while other parameters have constant values ($\alpha\Omega t = 0.75$, $\text{Re}_\alpha = 3.63$, and $\omega = 85.5$). These can be contrasted to two cases, which differ by $\pm 10\%$ in the value of Ω from the middle case (the dashed line has $\alpha\Omega t = 0.82$ and $\omega = 94.1$ and the dash-dotted line has $\alpha\Omega t = 0.67$ and $\omega = 77.0$). The vortices are shown in the rotating coordinate system.

with some, as yet unknown, function G_z . A similar analysis can be done for the azimuthal velocity, and the result can be written as

$$v_{L\phi} = (\alpha' - 1) R \Omega G_\phi \left(\frac{R^2 \Omega}{\kappa}, \frac{R}{a}, \frac{1 - \alpha'}{\alpha} \right) \quad (7)$$

with a function G_ϕ . Note that Eq. (7) is valid only in the rotating frame; the laboratory frame azimuthal velocity $v_{L\phi} + R\Omega$ does not have this form. Because the parameter $R^2\Omega/\kappa$ appears repeatedly, we define a dimensionless angular velocity:

$$\omega := \frac{2\pi R^2 \Omega}{\kappa}. \quad (8)$$

We also remind that the last parameter in Eqs. (6) and (7) has the short-hand $\text{Re}_\alpha \equiv (1 - \alpha')/\alpha$.

Another, in this case approximate, simplification is offered by the fact that \mathbf{v}_L has only a weak logarithmic dependence on R/a , see e.g., Refs. 31 and 32. Hence, different values of R/a have only a minor effect on the results; this is demonstrated in Fig. 3. Because of this weak dependence, we have fixed $R/a = 1.77 \times 10^5$ in all other calculations in this paper except in the ones presented in Fig. 7. We consider explicitly the case, where the lower end of the cylinder (small z side) is in a vortex state with positive circulation and the angular velocity Ω is positive. The case of negative circulation and negative angular velocity has the same v_{Lz} and opposite $v_{L\phi}$.

IV. CRITICAL ANGULAR VELOCITIES

Two critical angular velocities are important for our problem. They can be found analytically by studying the following expression of free energy F (per unit length) of the superfluid with an axially oriented vortex line displaced at the distance r from the cylinder axis:^{2,33,34}

$$F(r, \Omega) = \frac{\rho_s \kappa^2}{4\pi} \left[\ln \frac{R}{a} + \ln \left(1 - \frac{r^2}{R^2} \right) - \frac{2\pi R^2 \Omega}{\kappa} \left(1 - \frac{r^2}{R^2} \right) \right]. \quad (9)$$

This expression is valid when $a \ll R$.

In the order of increasing Ω , the first critical velocity Ω_m corresponds to an axial vortex becoming metastable. It can be obtained from the condition:

$$\left. \frac{\partial^2 F(r, \Omega_m)}{\partial r^2} \right|_{r=0} = 0. \quad (10)$$

($\partial F / \partial r = 0$ is automatically satisfied at $r = 0$ for all $\Omega \geq 0$.) This condition gives:

$$\Omega_m = \frac{\kappa}{2\pi R^2}. \quad (11)$$

In dimensionless form: $\omega_m \equiv (2\pi R^2 / \kappa) \Omega_m = 1$. This first critical angular velocity is analogous to a critical field in a type II superconductor, above which the so-called Bean-Livingston barrier³⁵ is created.

The second critical velocity Ω_s corresponds to a single axial vortex becoming absolutely stable, i.e. its free energy (8) becomes less than the Landau-state free energy $F = 0$. This leads to:

$$\Omega_s = \frac{\kappa}{2\pi R^2} \ln \frac{R}{a}. \quad (12)$$

In dimensionless form: $\omega_s \equiv 2\pi R^2 \Omega_s / \kappa = \ln(R/a)$, which in our case ($R/a = 1.77 \times 10^5$) has the value 12.08. The second critical angular velocity is an analog of the lower critical magnetic field, at which the phase transition between the Meissner state and the mixed state takes place in type II superconductors.

The one-vortex state loses absolute stability when the two-vortex state becomes stable^{33,34}, but it still remains metastable. The critical velocity v_c for vortex nucleation at the cylindrical wall limits the metastability of the one-vortex state to $\omega < \omega_c := 2\pi R v_c / \kappa$. We study below a wide range of ω , but the results are applicable only as long as ω remains below ω_c . For ³He-B in a vessel with smooth walls $\omega_c \gg 1$ can be achieved, which justifies the present study.

V. ASYMPTOTIC VORTEX VELOCITY IN A NON-TILTED CYLINDER

The evolution of the vortex is solved by numerically integrating Eq. (4) forward in time in the rotating frame. Our numerical scheme uses a half-infinite cylinder, but the results for the asymptotic velocity and the vortex form in an untilted

cylinder are equally valid for an infinite cylinder. For large rotation velocities we typically use a quarter vortex ring as our initial condition. The radius of the ring is half of the cylinder radius. The ring is situated so that the vortex starts from the bottom of the cylinder and ends at the cylinder wall. For small rotational velocities ($\Omega \lesssim \Omega_s$) the initial configuration was taken from previous iterations at somewhat larger Ω . This was necessary in order to reach the steady state quickly enough, or even in order to avoid the shrinking away of the initial configuration. Both ends of the vortex are allowed to move freely. Any vortex end touching the wall is always normal to it. In principle, a vortex line may also form a closed loop, without touching the boundary at all. A vortex loop may be created when a vortex line reconnects with itself. If a vortex loop comes very close to the wall, it reconnects with it, that is, snaps open, with the two vortex ends connecting to the wall orthogonally.

The use of a quarter vortex ring as the initial condition is not necessary. What matters is whether the required asymptotic evolution (if it exists) is reached from the initial condition or not, and a quarter ring is suitable in a large parameter range. However, if the temperature is low and the shape of the vortex is far from the asymptotic one, the vortex may oscillate a long time before reaching a stable form. For $\text{Re}_\alpha \gtrsim 100$, even the quarter ring vortex leads to long-lasting oscillations in the vortex shape.

Our goal is to study the velocity of the end point of the vortex \mathbf{v}_L (5). Before going to the general case, we consider some limiting cases where analytic solutions are found.

In the limit $\omega \gg 1$, the cylinder wall at $r = R$ can be thought of as a plane and we assume that the vortex line approaches the wall as a straight line normal to it. We can now put $\Omega = \Omega \hat{\mathbf{e}}_z$, $\mathbf{r} = R \hat{\mathbf{e}}_r$, a point on the large cylinder wall (or plane) and $\hat{\mathbf{s}}' = \hat{\mathbf{e}}_r$. This gives $\mathbf{v}_s = -R\Omega \hat{\mathbf{e}}_\phi$ in rotating coordinates, and inserting it into Eq. (4) we get:

$$\mathbf{v}_L = R\Omega [\alpha \hat{\mathbf{e}}_z + (\alpha' - 1) \hat{\mathbf{e}}_\phi]. \quad (13)$$

Hence $v_{Lz} = \alpha R\Omega$, $v_{L\phi} = (\alpha' - 1)R\Omega$, and $\tan \beta = -\text{Re}_\alpha^{-1}$.

Another exact result corresponds to vanishing velocity of the vortex line, $\mathbf{v}_L = 0$, at the critical angular velocity $\Omega = \Omega_s$ (12). Since at $\Omega = \Omega_s$ the one-vortex and no-vortex states are in equilibrium, there is no force to drive the vortex. Therefore at $\Omega = \Omega_s$ the vortex must be stationary in the rotating frame, for all temperatures $0 < T < T_c$.

A third special case is the limit $T \rightarrow 0$. In this limit the normal fluid component vanishes and thus the vortex does not feel the rotation of the container. Therefore the shape and the motion of the vortex, as measured in the laboratory coordinates, do not depend on the rotational velocity of the vessel. As the previous limiting case ($\Omega = \Omega_s$) extends to this limit as well, we expect that the shape of the vortex in the $T \rightarrow 0$ limit is the same as the equilibrium shape at $\Omega = \Omega_s$. This implies that the velocity in the laboratory system is $v_{Lz} = 0$ and $v_{L\phi} = R\Omega_s$. In the rotating frame these translate to $v_{Lz} = 0$ and $v_{L\phi} = R(\Omega_s - \Omega)$.

Based on these limiting cases, we can refine the depen-

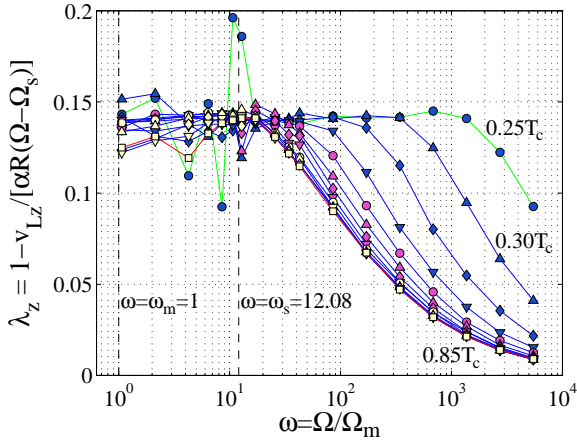


FIG. 4. (Color online) The axial velocity of the vortex v_{Lz} expressed by λ_z (14). The curves are plotted as a function of $\omega \equiv 2\pi R^2 \Omega / \kappa$. The used values of Re_α are given in Table I. They correspond approximately to temperatures $T/T_c = 0.25, 0.30, 0.35, \dots, 0.85$ in $^3\text{He-B}$. The two vertical dashed lines correspond to the two critical angular velocities Ω_m and Ω_s . The value of Ω_s used in calculating λ_z and λ_ϕ is an average obtained numerically from the calculated data: $\Omega_s = 12.55\Omega_m$, which deviates slightly from the theoretical value $\Omega_s = \ln(R/a)\Omega_m = 12.08\Omega_m$. Using this numerical value instead of the theoretical one eliminates a peak in λ_z and λ_ϕ near Ω_s that we believe to be a numerical artifact. The data still shows some numerical error, especially at low temperatures and for angular velocities $\Omega \approx \Omega_s$. The numerical calculation is consistent with the expectation that λ_z is a constant at $\Omega = \Omega_s$, and gives the value $\lambda_z \approx 0.14$.

dences (6) and (7) by introducing

$$v_{Lz} = \alpha R (\Omega - \Omega_s) (1 - \lambda_z), \quad (14)$$

$$v_{L\phi} = (\alpha' - 1) R (\Omega - \Omega_s) (1 - \lambda_\phi). \quad (15)$$

We have defined new dimensionless functions λ_z and λ_ϕ , which, similarly as G_z and G_ϕ , are functions of ω (8), R/a , and Re_α . The rationale here is that the λ functions are small compared to unity, so that a crude approximation can be obtained by neglecting λ_z and λ_ϕ in Eqs. (14) and (15). This already implies that the sign of v_{Lz} is determined by $\Omega - \Omega_s$: the vortex grows for $\Omega > \Omega_s$ and shrinks for $\Omega < \Omega_s$. The sign of $v_{L\phi}$ is determined similarly, but noting that the coefficient $\alpha' - 1$ is negative.

The numerically calculated asymptotic velocities v_{Lz} and $v_{L\phi}$ are shown in Figs. 4 and 5. The results are presented using the λ functions defined in Eqs. (14) and (15). The figures show some scatter especially for Ω close to Ω_s that arises from inaccuracies in the numerical calculation. In spite of this, we can conclude that the limiting cases mentioned above are consistent with the data. In particular, both λ_z and λ_ϕ are finite functions, which guarantees stationarity at $\Omega = \Omega_s$. Both λ_z and λ_ϕ approach zero in the limit of large ω . In the limit $T \rightarrow 0$, λ_ϕ approaches zero irrespective of ω . There is no restriction on λ_z in the limit $T \rightarrow 0$ since the prefactor $\alpha \rightarrow 0$ in Eq. (14).

From Figs. 4 and 5 one can see that both λ_z and λ_ϕ are

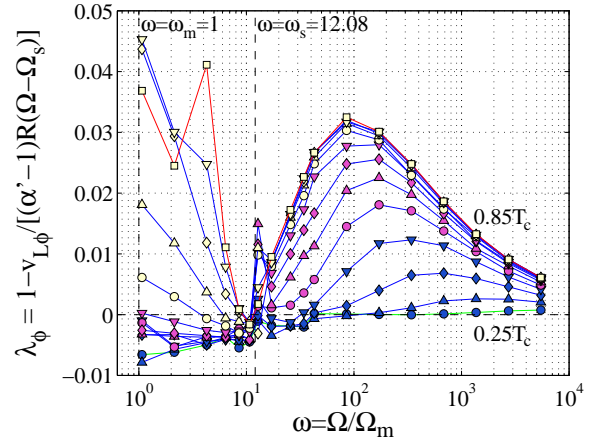


FIG. 5. (Color online) The azimuthal velocity of the vortex $v_{L\phi}$ in the rotating frame, expressed by λ_ϕ (15). The curves are plotted as a function of ω at the same values of the parameter Re_α as used in Fig. 4, again corresponding to approximate temperatures from $0.25T_c$ to $0.85T_c$ in $^3\text{He-B}$. The two vertical dashed lines correspond to the two critical angular velocities Ω_m and Ω_s . The value of Ω_s used for calculating λ_ϕ is the same as for λ_z in Fig. 4. Here also, numerical errors are prominent for low temperatures and for $\Omega \lesssim \Omega_s$. The numerical results are consistent with the expectation that λ_ϕ vanishes at $\Omega = \Omega_s$, and in the low temperature limit. The negative values of λ_ϕ most likely arise from numerical inaccuracy.

constants (independent of T) at $\Omega = \Omega_s$. This can be understood by considering the mutual friction as a small perturbation in the vicinity of $\Omega = \Omega_s$. As the mutual friction parameters appear explicitly in Eqs. (14) and (15), the functions λ_z and λ_ϕ should not depend on $(1 - \alpha')/\alpha$ at $\Omega = \Omega_s$. Generalizing this argument, we can say that around $\Omega = \Omega_s$ there is an *inertial regime*, where the vortex shape is dominated by non-dissipative forces. This regime is characterized by $\lambda_z \approx 0.14$. There is a complementary *dissipative regime*, where $\lambda_z \ll 0.14$. The boundary between the two is at $\Omega - \Omega_s \approx \text{Re}_\alpha \Omega_s$. Both the inertial and dissipative limits seem to correspond to vanishing λ_ϕ , but non-vanishing values appear in the cross-over regime.

We note that although the curves in Figs. 4 and 5 are labeled by temperature, the results are completely general. The temperatures correspond to different values of Re_α according to table I and the dependence on α or α' is through the scaling relations (6) and (7), or (14) and (15).

For large ω we can identify the approximate power laws

$$\begin{aligned} v_{Lz} &\simeq \alpha R \Omega [1 - (\Omega/\Omega_z)^{k_z}], \\ v_{L\phi} &\simeq (\alpha' - 1) R \Omega [1 - (\Omega/\Omega_\phi)^{k_\phi}]. \end{aligned} \quad (16)$$

Fitting in the range $\Omega \in [85\Omega_m, 5472\Omega_m]$ at $\text{Re}_\alpha = 0.083$ ($\sim 0.85T_c$) gives $k_z = -0.72$ and $\Omega_z = 10.6\Omega_m$. Fitting in the range $\Omega \in [684\Omega_m, 5472\Omega_m]$ at $\text{Re}_\alpha = 0.083$ ($\sim 0.85T_c$) gives $k_\phi = -0.71$ and $\Omega_\phi = 6.47\Omega_m$.

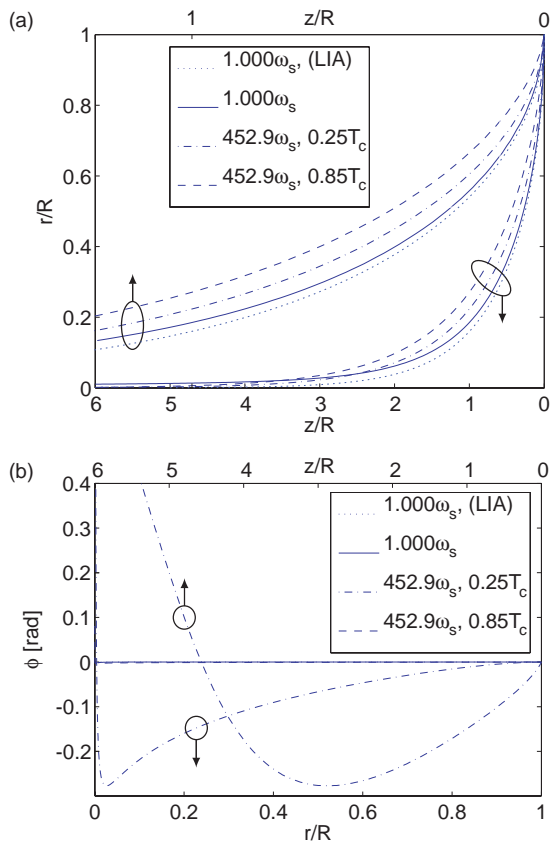


FIG. 6. (Color online) Asymptotic vortex shape. The different curves are for the equilibrium shape at $\omega = \omega_s$, for two temperatures ($T = 0.25T_c$ and $0.85T_c$) at a high rotation velocity ($\omega = 452.9\omega_s$) and for the equilibrium shape in the local induction approximation (LIA)¹⁸. It is expected that the same equilibrium shape as at $\omega = \omega_s$ is reached also in the low temperature limit $T \rightarrow 0$. a) r against z showing all four curves both with a unit aspect ratio (horizontal scale at top) and with a compressed z -scale (horizontal scale at bottom); b) ϕ against z (horizontal scale at top) and ϕ against r (horizontal scale at bottom). Out of the four cases, only one ($452.9\omega_s, 0.25T_c$) shows significant deviation from planar shape. In this figure $z = 0$ corresponds to the end of the vortex at $r = R$. The temperatures are approximative values for $^3\text{He-B}$, corresponding Re_α parameters in Table I. (The arrows indicate the scale corresponding to the curves.)

These results for the full Biot-Savart model can be compared with those for a local induction approximation^{3,36,37} (LIA) method, where the Biot-Savart integral (2) is replaced by a local term:

$$\mathbf{v}_\omega = \frac{\kappa}{4\pi} \ln\left(\frac{8}{e^{1/2}a|s''|}\right) \hat{\mathbf{s}}' \times \mathbf{s}'' \quad (17)$$

We have made numerical tests using this approximation. The main difference to the results above is that the effective value of Ω_s is increased by 5...7 per cent. An alternative form of LIA is to assume that the logarithmic factor in (17) is a constant, which then can be adjusted to reproduce the exact value of Ω_s ¹⁸. Even if the LIA model gives a suitable approximation for the velocities, it gives wrong results in some cases, an example being the prediction $\Omega_m = 0$.

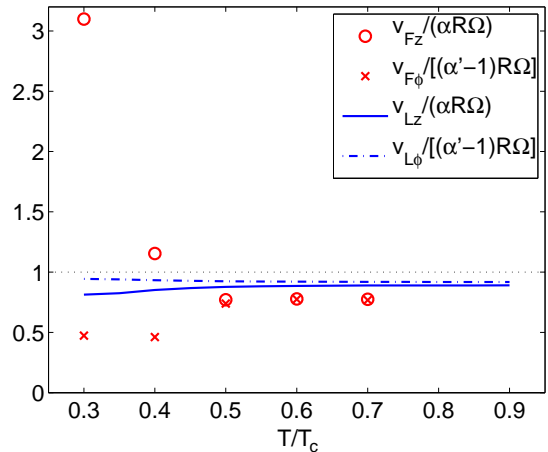


FIG. 7. (Color online) Comparison of numerically calculated asymptotic velocities between a single vortex end (v_{Lz} and $v_{L\phi}$) and a vortex front (v_{Fz} and $v_{F\phi}$). The lines are for a single vortex, giving the axial (solid line) and azimuthal (dash-dotted line) components. The data points are for the vortex front, giving the axial (circles) and the azimuthal velocities (crosses). All azimuthal velocities are in the rotating coordinate system. The front velocity is from numerical simulations, originally presented in Ref. 12, p. 3219. The parameters are $\omega = 213.8$ and $R/a = 0.88 \times 10^5$.

The shape of the top part of a rotating vortex is depicted in Fig. 6. The equilibrium shape at $\omega = \omega_s$ (solid line) is independent of the friction parameters, as discussed above. The equilibrium shape in the local induction approximation can be solved analytically if a constant cut-off radius is assumed¹⁸. This result (dotted line) slightly differs from the result of our numerical full Biot-Savart calculation. The most important difference in the vortex shape is that within the LIA model the vortex approaches the rotation axis exponentially, while the full Biot-Savart model gives slower convergence towards the rotation axis (possibly with some power law). This is due to vortex segments near $r \approx R$, which induce an azimuthal velocity field that vanishes slower than exponentially. Both of these structures lie in a single plane, i.e. ϕ as a function of z (or r) is a constant. At higher rotational velocity the shape of the vortex changes. In Fig. 6 the curve at $0.85T_c$ (dashed line) represents the dissipation-dominated case. In this limit the vortex is again confined to a plane. In the cross-over regime there are deviations from a plane, the curve at $0.25T_c$ (dash-dotted line) representing an extreme example.

The vortex shape can also be analyzed as follows. Once we know the line velocity from Figs. 4 and 5, we can invert the equation of motion (4) to find the transverse part of the superfluid velocity \mathbf{v}_s at the vortex line. We apply this to the end point of the vortex at the cylindrical wall ($r = R$), and find:

$$v_{s,z} = \frac{-\lambda_z + \lambda_\phi}{\text{Re}_\alpha^{-1} + \text{Re}_\alpha} R(\Omega - \Omega_s), \quad (18)$$

$$v_{s,\phi} = \left(\frac{\text{Re}_\alpha^{-1} \lambda_z + \text{Re}_\alpha \lambda_\phi}{\text{Re}_\alpha^{-1} + \text{Re}_\alpha} - 1 \right) R(\Omega - \Omega_s). \quad (19)$$

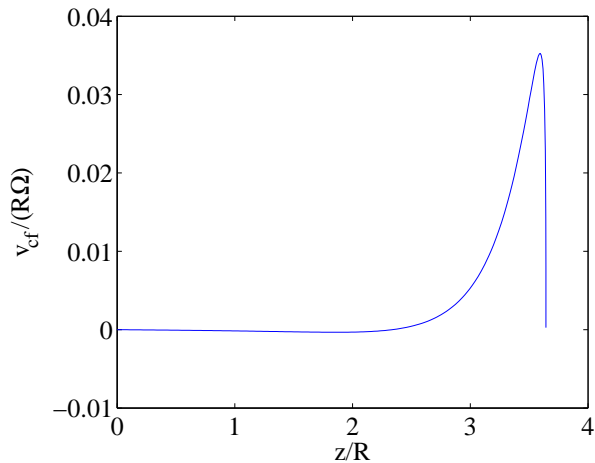


FIG. 8. (Color online) Value of counterflow projected on the vortex tangent, non-tilted cylinder. There is a clear peak near the top of the vortex, then a rapid drop to zero. The critical value of projected counterflow velocity for Kelvin waves with wavelength R is $v_{c,OG} = 0.1634R\Omega$, which is clearly not reached. The parameters are the same as for the last vortex state in Fig. 2a.

A non-zero $v_{s,z}$ can arise from the Biot-Savart integral (2) only if the vortex is not in a single plane. Thus the vortex can be planar only when the right-hand-side of Eq. (18) vanishes. This happens only in special cases such as $\Omega = \Omega_s$, or $T \rightarrow T_c$, or $T \rightarrow 0$, or $\omega \rightarrow \infty$.

The results above can be compared to the case of many vortices forming a vortex front. The comparison of the axial velocity is made in Fig. 7. The velocity of a moving front is affected by the twisting of vortices behind the front. An analytic formula has been applied to analyze the effect of this twisting on the front velocity^{16,38}. What is studied in this paper could be termed as the single vortex contribution to the vortex front velocity; twisting of vortices adds another contribution, surface friction yet another, and phenomena associated with turbulence (reconnections, Kelvin cascade, vortex tangle diffusion), yet another. Understanding the motion of such a vortex front is an open problem. In particular, experiments seem to indicate that a vortex front has a nonzero propagation velocity even in the zero-temperature limit. This cannot be fully explained by our filament model, which lacks a mechanism of dissipating free energy at zero temperature.

However, such a mechanism that changes the free energy in the low temperature limit (a necessity to sustain the propagation of a vortex, or of a vortex front) may be provided by the pinning of vortices to the container wall. This pinning can be seen as an effective surface friction, pumping energy into, or out of, the system. Also, the quasiparticle states in the vortex cores may transfer energy between the fluid and the container, when the vortex is attached to the wall.

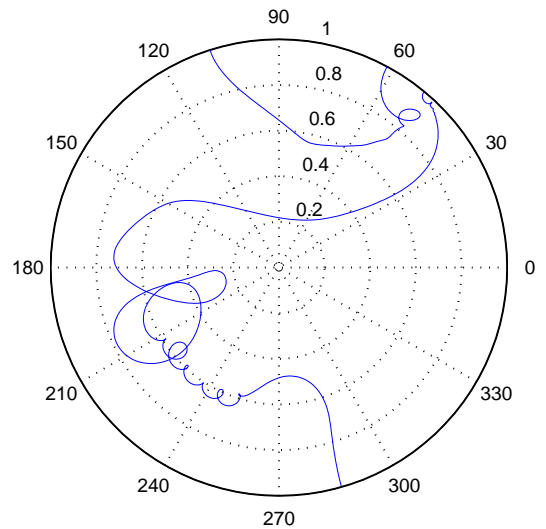


FIG. 9. (Color online) Kelvin waves created in a rotating tilted cylinder. The appearance of Kelvin waves, (which can be clearly seen in the lower left quadrant of the polar plot) is due to Ostermeier-Glaberson instability caused by the background velocity field \mathbf{v}_b . This background velocity field is nonzero in a rotating tilted cylinder and in this case causes a sufficiently strong counterflow along the vortex line to create Kelvin waves. The parameters are $\alpha\Omega t = 0.56$, $\text{Re}\alpha = 20.6$ ($\sim 0.3T_c$ in $^3\text{He-B}$), $2\pi R^2\Omega/\kappa = 85.5$, and $\theta = 60^\circ$.

VI. STABILITY OF VORTICES

Our numerical calculations indicate that once we have a vortex, whose end moves upwards, it is found to be stable at all temperatures, even in the zero temperature limit. This is somewhat surprising, since the previous simulations and experimental studies in $^3\text{He-B}$ have indicated that below a certain temperature, roughly $0.5T_c$ (or $\text{Re}\alpha \gtrsim 1.5$), a single vortex becomes unstable^{13,23,39}. We suggest that this kind of single vortex instability is due to some surface effects (such as pinning), or heat leaks causing extra counterflow. Earlier simulations, which also neglected surface friction, additionally assumed a cubical container instead of a cylindrical one²³. Studies of a decaying vortex array (spin-down)⁴⁰, also indicate that vortices in a cylindrical container are much more stable than vortices in a cubical one.

Another source of instability is related to the creation and growth of Kelvin waves. The so-called Ostermeier-Glaberson instability^{41,42} appears when the counterflow $\mathbf{v}_{cf} := \mathbf{v}_n - \mathbf{v}_s$ along the vortex line is sufficiently strong, and causes straight vortex lines to become unstable towards the appearance of Kelvin waves. For a single axially oriented straight vortex, the critical counterflow velocity, above which the amplitude of Kelvin waves with a wave vector k are able to grow, is:

$$v_{c,OG} = \frac{\Omega + \eta k^2}{k}, \text{ where } \eta = \frac{\kappa}{4\pi} \ln \frac{1}{ka}. \quad (20)$$

In our case of a non-tilted cylinder with a vortex attached to the cylinder wall this effect may exist in some situations. From Fig. 2b one observes that the vortex has a small com-

ponent along the azimuthal direction. This results in a non-zero counterflow along the vortex and could in principle cause Ostermeier-Glaberson instability.

However, growing Kelvin waves are not observed in simulations when the tilt is absent. The reason becomes apparent if one looks at Fig. 8, where we have plotted the counterflow along the vortex. The counterflow along the vortex line has its maximum in the top part of the vortex and falls sharply below it. Near the axis it is practically zero. The maximum value for the counterflow indicates that the Kelvin waves that could grow have a wavelength much longer than the cylinder radius, and, therefore, larger than the region of this finite counterflow. Hence, the Kelvin waves cannot grow and Ostermeier-Glaberson instability does not play any role.

In contrast, the situation in a tilted rotating cylinder is different. With enough tilting, the boundary superfluid velocity v_b creates a sufficiently strong counterflow, which results in the appearance of Kelvin waves. These Kelvin waves then produce a change from a laminar to a more turbulent fluid motion, possibly resulting in a vortex tangle, see Fig. 9. Yet another phenomenon is the Crow instability⁴³ which applies to vortices that are close to each other, or close to the wall (which can be interpreted as being close to the image vortex). This instability is due to the fact that vortices of opposite direction attract each other. Thus, the parts of vortices that are slightly closer to each other start moving faster towards each other, deforming the vortices even more, and eventually resulting in a large number of reconnections and new vortices. In our case the Crow instability does not work in the untilted cylinder since the rotation provides a stabilizing effect.

VII. EFFECT OF TILTING

Tilting the vessel has the advantage of breaking the cylindrical symmetry. A small tilt may be useful in calculations also for detecting effects that occur due to this asymmetry, unavoidably present in experimental situations.

The most prominent effect caused by the tilt is, as noted above, the instability of the vortex. At low temperatures and for a large tilt, several initial configurations (at large enough rotation) lead to growing Kelvin waves and eventually to a creation of a vortex tangle via reconnections. However, with an initial state close to the steady state, the vortex smoothly adopts its new asymptotic form and no new vortices are generated.

A second noticeable effect of tilting is the oscillation of v_{Lz} about a constant value (close to $\alpha R \Omega \cos \theta$). This is due to a sinusoidal component of the boundary field²⁵.

A somewhat surprising effect was also found. At a large enough tilt angle the azimuthal velocity of the vortex end may approach zero (in moving coordinates). Thus, in the asymptotic limit, the vortex end becomes locked at some azimuthal angle, while a constant axial velocity component remains. A detailed study of this phenomenon has not been done yet, but this sort of behavior can be seen in the last two pictures of Fig. 10, corresponding to tilting angles 50° and 60° .

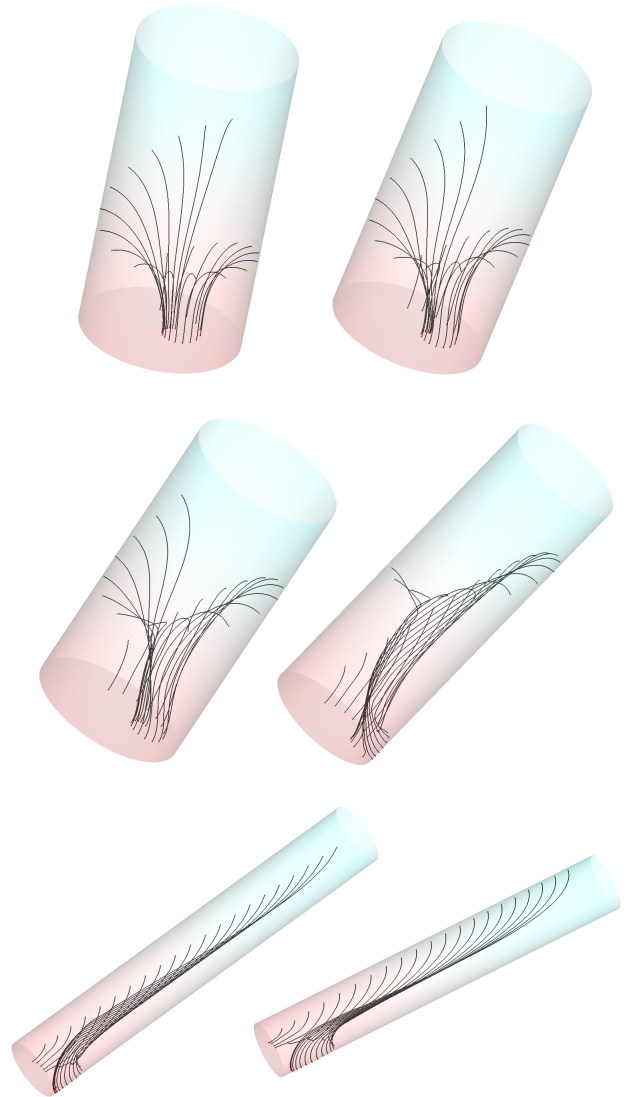


FIG. 10. (Color online) Vortex evolution for different tilting angles. Twenty-one snapshots are shown for each tilting with angles $\theta = 10^\circ, 20^\circ, 30^\circ, 40^\circ, 50^\circ, \text{ and } 60^\circ$. With increasing tilting some qualitative differences appear. The starting point of the vortex may climb on the side wall. The end point may start moving axially. All plots are in the rotating coordinate system. The total time is $2.33/\alpha\Omega$, $\text{Re}_\alpha = 3.63$, and $\omega = 85.5$.

VIII. CONCLUSIONS

While one could say that we have been “hitting a mosquito with a cannonball”, using a code created for brute force large scale vortex tangle calculations to do a very simple job, there still is, we believe, some potentially useful information to be gained from this endeavor.

Vortex motion in a cylinder with smooth walls was found to be quite stable, both in the untilted and moderately tilted ($\lesssim 30^\circ$) cases. This limits the causes for the experimentally observed single vortex instability^{13,23,39} to areas not covered

in this study, such as surface effects and heat flows.

In our ideal cylindrical environment, vortex motion can be estimated by considering the limiting cases at $T \rightarrow 0$, $\Omega = \Omega_s$, and $\Omega \rightarrow \infty$. In a more general case the correct motion can be characterized by introducing a small correction to these limiting cases. Our scaling argument additionally emphasizes that this correction depends only on the dimensionless parameters $R^2\Omega/\kappa$, Re_α , and R/a , the last dependence being weak (logarithmic). At large enough rotational velocities the vortex motion is dominated by *dissipative* effects. Near Ω_s one may observe an *inertial regime* where non-dissipative forces dominate. In general, the asymptotic vortex shape is three-dimensional, but e.g., at $\Omega = \Omega_s$ the vortex configuration is confined to a plane. Deviations from the plane structure are typically small, the largest deviations appearing at low temperatures, and with relatively large rotation velocities.

This study highlights the role of scaling properties in superfluids and other analogous systems. A deeper analysis to connect these formulas to the velocity of the vortex front should be carried out. The azimuthally locked motion in the tilted case was an unexpected result.

ACKNOWLEDGMENTS

We would like to express our gratitude to Professor Alexander L. Fetter for useful comments and discussions. This work is supported by the Academy of Finland and EU 7th Framework Programme (FP7/2007-2013, grant 228464 MikrocKelvin).

- ¹ R. P. Feynman, in *Prog. Low Temp. Phys.*, Vol. 1, edited by C. J. Gorter (Elsevier, 1955) pp. 17–53.
- ² A. L. Fetter, *Phys. Rev.* **138**, A429 (1965).
- ³ K. W. Schwarz, *Phys. Rev. B* **31**, 5782 (1985).
- ⁴ E. B. Sonin, *Rev. Mod. Phys.* **59**, 87 (1987).
- ⁵ R. Donnelly, *Quantized Vortices in Helium II* (Cambridge University Press, 1991).
- ⁶ M. Tsubota, T. Araki, and S. K. Nemirovskii, *J. Low Temp. Phys.* **119**, 337 (2000).
- ⁷ C. F. Barenghi, R. J. Donnelly, and W. F. Vinen, eds., *Quantized Vortex Dynamics and Superfluid Turbulence* (Springer, 2001).
- ⁸ W. F. Vinen and J. J. Niemela, *J. Low Temp. Phys.* **128**, 167 (2002).
- ⁹ D. Kivotides and A. Leonard, *Phys. Rev. Lett.* **90**, 234503 (2003).
- ¹⁰ M. Tsubota, T. Araki, and C. F. Barenghi, *Phys. Rev. Lett.* **90**, 205301 (2003).
- ¹¹ M. Tsubota, C. F. Barenghi, T. Araki, and A. Mitani, *Phys. Rev. B* **69**, 134515 (2004).
- ¹² A. P. Finne, V. B. Eltsov, R. Hänninen, N. B. Kopnin, J. Kopu, M. Krusius, M. Tsubota, and G. E. Volovik, *Rep. Prog. Phys.* **69**, 3157 (2006).
- ¹³ V. B. Eltsov, R. de Graaf, R. Hänninen, M. Krusius, R. E. Solntsev, V. S. L'vov, A. I. Golov, and P. M. Walmsley, in *Prog. Low Temp. Phys.*, Vol. 16, edited by W. B. Halperin and M. Tsubota (Elsevier, 2009) Chap. 2, pp. 45–146.
- ¹⁴ A. W. Baggaley and C. F. Barenghi, *Phys. Rev. B* **84**, 020504 (2011).
- ¹⁵ R. Hänninen, A. Mitani, and M. Tsubota, *J. Low Temp. Phys.* **138**, 589 (2005).
- ¹⁶ V. B. Eltsov, A. P. Finne, R. Hänninen, J. Kopu, M. Krusius, M. Tsubota, and E. V. Thuneberg, *Phys. Rev. Lett.* **96**, 215302 (2006).
- ¹⁷ R. Hänninen, V. B. Eltsov, A. P. Finne, R. de Graaf, J. Kopu, M. Krusius, and R. E. Solntsev, *J. Low Temp. Phys.* **155**, 98 (2009).
- ¹⁸ E. B. Sonin and S. K. Nemirovskii, *Phys. Rev. B* **84**, 054506 (2011).
- ¹⁹ R. J. Zieve, Yu. Mukharsky, J. D. Close, J. C. Davis, and R. E. Packard, *Phys. Rev. Lett.* **68**, 1327 (1992).
- ²⁰ T. Sh. Misirpashaev and G. E. Volovik, *JETP Lett.* **56**, 41 (1992).
- ²¹ K. W. Schwarz, *Phys. Rev. B* **47**, 12030 (1993).
- ²² E. B. Sonin, *J. Low Temp. Phys.* **97**, 145 (1994).
- ²³ A. P. Finne, T. Araki, R. Blaauwgeers, V. B. Eltsov, N. B. Kopnin, M. Krusius, L. Skrbek, M. Tsubota, and G. E. Volovik, *Nature* **424**, 1022 (2003).
- ²⁴ We use the core radius parameter a and the corresponding cut-off procedure in the sense that the velocity of a vortex ring in our calculations equals (within numerical error) the velocity of a vortex ring with a hollow core in a classical ideal fluid. See Ref. 5, pages 22-23 for how different core models relate to the velocity of a classical vortex ring.
- ²⁵ R. Hänninen, *J. Low Temp. Phys.* **156**, 145 (2009).
- ²⁶ T. D. C. Bevan, A. J. Manninen, J. B. Cook, H. Alles, J. R. Hook, and H. E. Hall, *J. Low Temp. Phys.* **109**, 423 (1997).
- ²⁷ H. E. Hall, *J. Phys.: Condens. Matter* **11**, 7677 (1999).
- ²⁸ G. E. Volovik, *JETP Lett.* **78**, 553 (2003).
- ²⁹ N. B. Kopnin, *Phys. Rev. Lett.* **92**, 135301 (2004).
- ³⁰ We would like to point out that this scaling property is independent of the shape of the container. The scaling property fails, when the field \mathbf{v}_b is not constant in time, unless its speed of time variation is also scaled by the factor α .
- ³¹ C. E. Swanson and R. J. Donnelly, *J. Low Temp. Phys.* **61**, 363 (1985).
- ³² K. W. Schwarz, *Phys. Rev. B* **38**, 2398 (1988).
- ³³ G. B. Hess, *Phys. Rev.* **161**, 189 (1967).
- ³⁴ L. J. Campbell and R. M. Ziff, *Phys. Rev. B* **20**, 1886 (1979).
- ³⁵ C. P. Bean and J. D. Livingston, *Phys. Rev. Lett.* **12**, 14 (1964).
- ³⁶ L. S. Da Rios, *Rend. Circ. Mat. Palermo* **22**, 117 (1906).
- ³⁷ R. J. Arms and F. R. Hama, *Phys. Fluids* **8**, 553 (1965).
- ³⁸ V. B. Eltsov, R. de Graaf, R. Hänninen, M. Krusius, and R. E. Solntsev, *J. Low Temp. Phys.* **150**, 373 (2008).
- ³⁹ A. P. Finne, V. B. Eltsov, G. Eska, R. Hänninen, J. Kopu, M. Krusius, E. V. Thuneberg, and M. Tsubota, *Phys. Rev. Lett.* **96**, 085301 (2006).
- ⁴⁰ V. B. Eltsov, R. de Graaf, P. J. Heikkinen, J. J. Hosio, R. Hänninen, M. Krusius, and V. S. L'vov, *Phys. Rev. Lett.* **105**, 125301 (2010).
- ⁴¹ W. I. Glaberson, W. W. Johnson, and R. M. Ostermeier, *Phys. Rev. Lett.* **33**, 1197 (1974).
- ⁴² R. M. Ostermeier and W. I. Glaberson, *J. Low Temp. Phys.* **21**, 191 (1975).
- ⁴³ S. C. Crow, *AIAA Journal* **8**, 2172 (1970).